

Synthesis of Cationic Rhenium(VII) Oxo Imido Complexes and Their Tunability Towards Oxygen Atom Transfer

Elon A. Ison,[†] Jeanette E. Cessarich, Nicholas E. Travia, Phillip E. Fanwick, and Mahdi M. Abu-Omar*

Contribution from the Brown Laboratory, Department of Chemistry, Purdue University, 560 Oval Drive, West Lafayette, Indiana 47907

Received August 1, 2006; E-mail: mabuomar@purdue.edu

Abstract: A facile method is described for the synthesis of cationic Re(VII) *cis* oxo imido complexes of the form [Re(O)(NAr)(salpd)⁺] (salpd = *N,N*-propane-1,3-diybis(salicylideneimine)), **4**, [Re(O)(NAr)(saldach)⁺] (saldach = *N,N*-cyclohexane-1,3-diybis(salicylideneimine)), **5**, and [Re(O)(NAr)(hoz)₂⁺] (hoz = 2-(2'-hydroxyphenyl)-2-oxazoline) (Ar = 2,4,6-(Me)₃C₆H₂; 4-(OMe)₂C₆H₃; 4-(Me)₂C₆H₃; 4-(CF₃)₂C₆H₃; 4-MeC₆H₄-SO₂), **6**, from the reaction of oxorhenium(V) [(L)Re(O)(Solv)⁺] (**1–3**) and aryl azides under ambient conditions. Unlike previously reported cationic Re(VII) dioxo complexes, these cationic oxo imido complexes can be obtained on a preparative scale, and an X-ray crystal structure of [Re(O)(NMe)(saldach)⁺], **5a**, has been obtained. Despite the multiple stereoisomers that could arise from tetradentate ligation of salen ligands to rhenium, one major isomer is observed and isolated in each instant. The electronic rationalization for stereoselectivity is discussed. Investigation of the mechanism suggests that the reactions of Re(V) with aryl azides proceed through an azido adduct similar to the group 5 complexes of Bergman and Cummins. Treatment of the cationic oxo imido complexes with a reductant (PAr₃, PhSMe, or PhSH) results in oxygen atom transfer (OAT) and the formation of cationic Re(V) imido complexes. [(salpd)Re(NMe)(PPh₃)⁺] (**7**) and [(hoz)₂Re(NAr)(PPh₃)⁺] (Ar = *m*-OMe phenyl) (**9**) have been isolated on a preparative scale and fully characterized including an X-ray single-crystal structure of **7**. The kinetics of OAT, monitored by stopped-flow spectroscopy, has revealed rate saturation for substrate dependences. The different plateau values for different oxygen acceptors (Y) provide direct support for a previously suggested mechanism in which the reductant forms a prior-equilibrium adduct with the rhenium oxo (Re^{VII} = O←Y). The second-order rate constants of OAT, which span more than 3 orders of magnitude for a given substrate, are significantly affected by the electronics of the imido ancillary ligand with electron-withdrawing imidos being most effective. However, the rate constant for the most active oxo imido rhenium(VII) is 2 orders of magnitude slower than that observed for the known cationic dioxo Re(VII) [(hoz)₂Re(O)₂⁺].

The use of heptavalent rhenium oxo complexes as oxidation catalysts has been extensively developed during the past 15 years. Particularly noteworthy is the chemistry of methylrhenium trioxide (MTO) which has found wide use in oxidation catalysis.¹ Because of the success of MTO, catalyst systems derived from this molecule have been of interest for a wide variety of transformations. Research activity in recent years has focused on inorganic and/or organometallic derivatives of MTO primarily possessing the LReO₃ trioxo core (where L is an anionic ligand).² In contrast, less research has involved the use of the cationic *cis* dioxo rhenium(VII) [L₂ReO₂⁺] framework. In these complexes, the high oxidation state combined with the cationic charge results in these species being very reactive. An example of this enhanced reactivity can be seen in the chemistry of the *cis* dioxo Re(VII) cations [{HB(pz)₃Re(O)₂R}⁺] (R = Ph,

Et, or Bu; and HB(pz)₃ = tris(pyrazolyl)borate) where the first example of the thermal migration of a ligand from a metal center to an oxo ligand has been observed.³ We have also shown the cationic Re(VII) dioxo complex [Re(O)₂(hoz)₂⁺] (hoz = 2-(2'-hydroxyphenyl)-2-oxazoline) to be a catalyst for the reduction of perchlorate via an oxygen atom transfer mechanism.⁴ These two cases are the only reported examples of characterizable cationic *cis* dioxo rhenium(VII) complexes, [L₂Re(O)₂⁺]. However, in both cases, the complexes were generated in situ and not isolated.⁵

[†] Present address: Department of Chemistry, North Carolina State University, Campus Box 8204, Raleigh, NC 27695.

(1) (a) Ramao, C. C.; Kuhn, F. E.; Herrmann, W. A.; *Chem. Rev.* **1997**, *97*, 3197–3246 and references therein. (b) Espenson, J. H. *Chem. Commun.* **1999**, 479–488. (c) Owens, G. S.; Arias, J.; Abu-Omar, M. M. *Catal. Today* **2000**, *55*, 317–363.

- (2) Representative examples of the LReO₃ motif: (a) Toganoh, M.; Ikeda, S.; Furuta, H. *Chem. Commun.* **2005**, 4589–4591. (b) Hegetschweiler, K.; Egli, A.; Herdtweck, E.; Herrmann, W. A.; Alberto, R.; Gramlich, V. *Helv. Chim. Acta* **2005**, *88*, 426–434. (c) Shan, X.; Ellern, A.; Espenson, J. H. *Angew. Chem., Int. Ed.* **2002**, *41*, 3807–2809. (d) Deubel, D. V.; Frenking, G. *J. Am. Chem. Soc.* **1999**, *121*, 2021–2031. (e) Herrmann, W. A.; Ding, H.; Kuehn, F. E.; Scherer, W. *Organometallics* **1998**, *17*, 2751–2757. (f) Gable, K. P.; Juliette, J. J. J.; Li, C.; Nolan, S. P. *Organometallics* **1996**, *15*, 5250–5251. (g) Paulo, A.; Domingos, A.; Marcalo, J.; Pires de Matos, A.; Santos, I. *Inorg. Chem.* **1995**, *34*, 2113–2120.
- (3) Brown, S. N.; Mayer, J. M. *J. Am. Chem. Soc.* **1996**, *118*, 12119–12133.
- (4) McPherson, L. D.; Drees, M.; Khan, S. I.; Strassner, T.; Abu-Omar, M. M. *Inorg. Chem.* **2004**, *43*, 4036–4050.

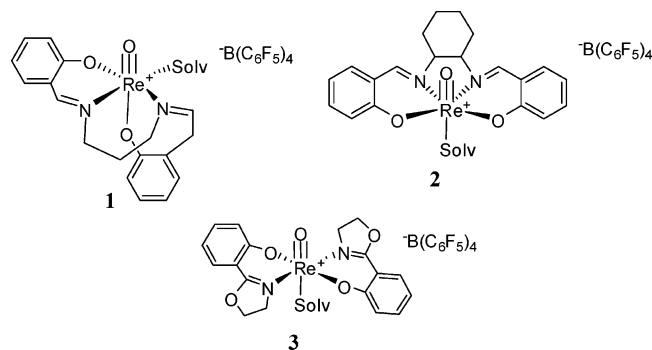


Figure 1. Cationic oxorhenium salen and oxazoline complexes 1–3.

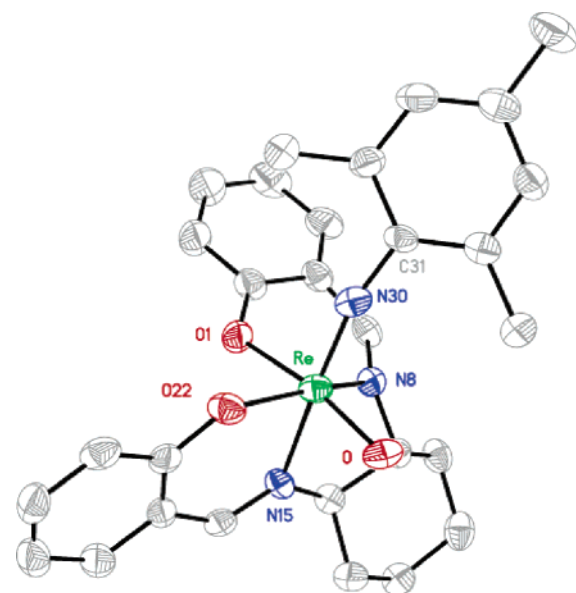


Figure 2. X-ray single-crystal structure of [(saldach)Re(O)(NMe)s]⁺[B(C₆F₅)₄][−], **5a**. Thermal ellipsoids are 50%. Hydrogens and the anion [B(C₆F₅)₄][−] have been removed for clarity. Selected bond distances (Å) and angles (deg). Re–O, 1.714(3); Re–O1, 2.052(3); Re–O22, 1.914(3); Re–N8, 2.070(4); Re–N15, 2.192(4); Re–N30, 1.751(4); N30–C31–Re, 164.7(3); O–Re–N30, 100.9(2); O–Re–O22, 102.0(2); N30–Re–O22, 103.3(2); O–Re–O1, 163.4(1); N30–Re–O1, 93.5(2); O22–Re–O1, 82.5(1); O–Re–N8, 90.0(2); N30–Re–N8, 94.0(2); O22–Re–N8, 156.5(2); O1–Re–N8, 80.6(1); O–Re–N15, 82.3(2); N30–Re–N15, 168.0(2); O22–Re–N15, 87.2(1); O1–Re–N15, 81.9(1); N8–Re–N15, 74.3(1).

A natural complement to this class of compounds is complexes possessing the oxo-imido framework [L₂Re(O)(NR)⁺].⁶ The tunable electronic properties of the imido ligand combined with the ability to vary its steric bulk are expected to provide complexes that are interesting to study in the context of atom transfer reactions. However, the synthesis and reactivity of these complexes until now have not been reported.

One common approach for the synthesis of imido complexes involves the decomposition of organic azides with the formation of dinitrogen as a byproduct.⁷ The mechanism for these reactions

is believed to involve an organo-azido intermediate, and in two cases metal-azido complexes have been isolated.⁸ Recently, we reported yet another mechanism for the reaction of organic azides with Mn(III) corroles that does not involve organo-azido intermediates; rather, the metal complex reacts with a transitory triplet nitrene generated upon thermolytic or photolytic activation of selected aryl azides.⁹ The use of aryl azides to generate transition metal imidos is of interest because metal imides have been implicated as active intermediates in group transfer catalysis.¹¹

As part of our continuing studies on the interactions of transition metals with organic azides, we investigated the reactions of the cationic oxorhenium salen complexes, [(salpd)Re(O)(Solv)]+[B(C₆F₅)₄][−] (**1**),¹² and [(saldach)Re(O)(Solv)]+[B(C₆F₅)₄][−] (**2**),¹² and the mono-oxo oxazoline complex [(hoz)₂Re(O)(Solv)]+[B(C₆F₅)₄][−] (**3**)¹³ (Figure 1). Herein we report the synthesis and full characterization of novel cationic rhenium(VII) oxo-imido complexes obtained from reactions with aryl azides under ambient conditions. We also examine the effect that systematic variation of the electronic properties of the imido ligand has on the oxidizing ability of these complexes. The reaction rates for oxygen atom transfer (OAT) from [Re^{VII}(O)(NR)⁺] to acceptor substrates have been measured and compared to those of the isoelectronic dioxo complex [(hoz)₂Re(O)₂]⁺. This study illustrates the ancillary ligand effect of imido [NR] vs oxo [O] on OAT reactions.

Results and Discussion

Synthesis of Cationic Rhenium(VII) Oxo Imido Complexes. Treatment of the cationic oxorhenium complexes **1–3** with 1 equiv of an aryl azide results in an immediate color change from green to red and the formation of the cationic oxo imido rhenium complexes **4–6** (Scheme 1). ¹H and ¹³C NMR spectra are consistent with a *cis* orientation of the imido and oxo ligands. The 2,4,6-trimethyl phenyl (mesityl) imido complexes with the salen-type ancillary ligands, **4** and **5a**, feature equivalent *ortho*-methyl groups in their ¹H spectra (δ 2.6, 6H), indicative of free rotation in solution about the N–C_{Ar} bond. In contrast, the mesityl imido complex of oxazoline, **6a**, displays two *ortho*-methyl peaks in the ¹H spectrum (δ 3.04, 3H and 2.80, 3H) at room temperature. The two methyl peaks coalesce in the VT-NMR experiment at 80 °C. The synthesis of complexes **4–6** from aryl azides is attractive because (1) the

(5) A search of the Cambridge Structural Database (CSD) of rhenium dioxo complexes yielded 413 hits of which 25 are rhenium(VII) dioxo and none of the 25 structures is cationic.

(6) A search of the Cambridge Structural Database (CSD) of rhenium oxo imido complexes afforded only four structures of rhenium(VII): Herrmann, W. A.; Ding, H.; Kuhn, F. E.; Scherer, W. *Organometallics* **1998**, *17*, 2751. (b) Guiterrez, A.; Wilkinson, G.; Hussain-Bates, B.; Hursthouse, M. B. *Polyhedron* **1990**, *9*, 2081. (c) Roesky, H. W.; Hesse, D.; Bohra, R.; Noltemeyer, M. *Chem. Ber.* **1991**, *124*, 1913.

(7) (a) Nugent, W. A.; Mayer, J. M. *Metal-Ligand Multiple Bonds*; Wiley: New York, 1988. (b) Wigley, D. E. *Prog. Inorg. Chem.* **1994**, *42*, 239.

(8) (a) Proulx, G.; Bergman, R. G. *Organometallics* **1996**, *15*, 684–692. (b) Proulx, G.; Bergman, R. G. *J. Am. Chem. Soc.* **1995**, *117*, 6382–6383. (c) Fickes, M. G.; Davis, W. M.; Cummins, C. C. *J. Am. Chem. Soc.* **1995**, *117*, 6384–6385.

(9) Abu-Omar, M. M.; Shields, C. E.; Edwards, N. E.; Eikey, R. A. *Angew. Chem., Int. Ed.* **2005**, *44*, 6203–6207.

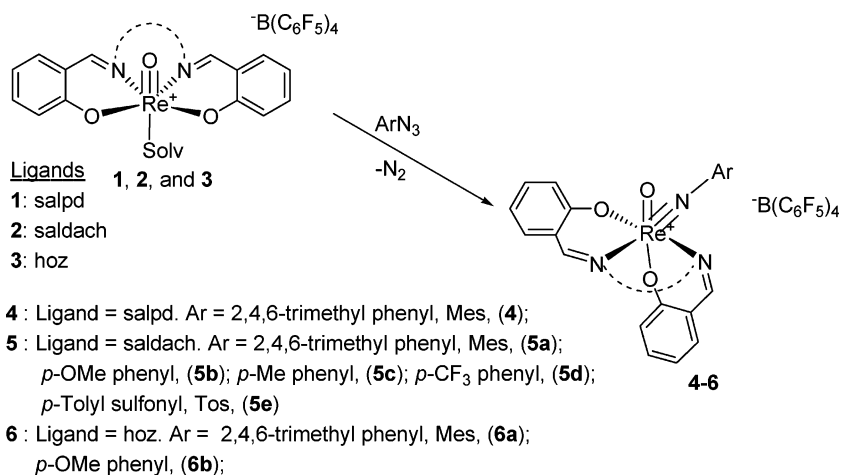
(10) (a) Groves, J. T.; Takahashi, T. *J. Am. Chem. Soc.* **1983**, *105*, 2073–2074. (b) Eikey, R. A.; Abu-Omar, M. M. *Coord. Chem. Rev.* **2003**, *243*, 83–124.

(11) Examples of the reactions of organic azides with transition metals: (a) Hu, X.; Mayer, K. *J. Am. Chem. Soc.* **2004**, *126*, 16322–16323. (b) Brown, S. D.; Betley, T. A.; Peters, J. C. *J. Am. Chem. Soc.* **2003**, *125*, 322–323. (c) Walstrom, A.; Pink, M.; Yang, X.; Tomaszewski, J.; Baik, M.-H.; Caulton, K. G. *J. Am. Chem. Soc.* **2005**, *127*, 5330–5331. (d) Lucas, R. L.; Powell, D. R.; Borovik, A. S. *J. Am. Chem. Soc.* **2005**, *127*, 11596–11597. (e) Jenkins, D. M.; Betley, T. A.; Peters, J. C. *J. Am. Chem. Soc.* **2002**, *124*, 11238–11239. (f) Mindiola, D. J.; Hillhouse, G. L. *J. Am. Chem. Soc.* **2001**, *123*, 4623–4624. (g) Mindiola, D. J.; Hillhouse, G. L. *Chem. Commun.* **2002**, 1840–1841.

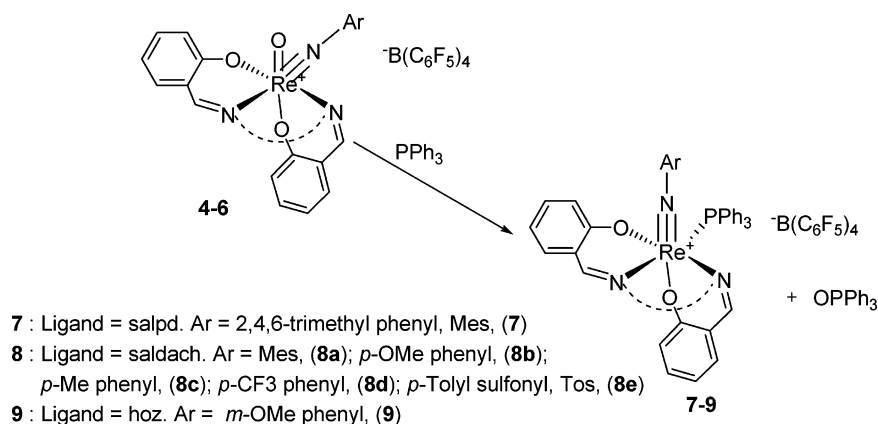
(12) Ison, E. A.; Cessarich, J. E.; Du, G.; Fanwick, P. E.; Abu-Omar, M. M. *Inorg. Chem.* **2006**, *45*, 2385–2387.

(13) (a) Ison, E. A.; Corbin, R. A.; Abu-Omar, M. M. *J. Am. Chem. Soc.* **2005**, *127*, 11938–11939. (b) Ison, E. A.; Trivedi, R. E.; Corbin, R. A.; Abu-Omar, M. M. *J. Am. Chem. Soc.* **2005**, *127*, 15374–15375.

Scheme 1



Scheme 2



reaction proceeds cleanly at ambient conditions requiring no thermal or photochemical activation of the organic azide, (2) the reactions proceed with moderate to high yields (70–90%), and (3) the only byproduct is molecular nitrogen (N₂), which simplifies isolation and purification as there are no organic side products to separate from the rhenium complexes.

X-ray Molecular Structure of [(saldach)Re(O)(NMes)]- $[\text{B}(\text{C}_6\text{F}_5)_4]$. Suitable crystals were obtained for X-ray diffraction by vapor diffusion of pentane into a concentrated methylene chloride solution of **5a** at room temperature (Figure 2). Complex **5a** adopts a distorted octahedral geometry with the angles around Re ranging from 74° to 168°. The Re imido bond is linear Re–N30–C31 (164.7(3)°) and the Re imido, Re–N30 (1.751(4) Å) and Re oxo, Re–O (1.714(3) Å) bond lengths are within normal range for Re–(heteroatom) multiple bonds.^{1,6,7} The Re oxo bond length is similar to that of the starting cationic oxo Re(V) complex **2**.¹² Bonds *trans* to multiply bonded ligands are significantly lengthened (Re–O1 (2.052(3) Å) *trans* to oxo and Re–N15 (2.192(4) Å) *trans* to imido) per the *trans* influence expected for multiply bonded ligands.

While there have been many structural examples of *tris*-oxo, *tris*-imido, *bis*-oxo imido, and *bis*-imido oxo congeners of MTO,¹⁴ examples of *cis* dioxo Re(VII) and their oxo imido or *bis*-imido analogues are rare.¹⁵ Hence, cationic derivatives of these complexes have not been isolated and structurally characterized. In fact, only two examples of cationic Re(VII) dioxo complexes have been generated and detected in situ but have not been structurally characterized.^{3,4} Complex **5** is the

only example to our knowledge of a structurally characterized cationic *cis* oxo-imido Re(VII) complex. Its synthesis allows us to compare its reaction chemistry directly to the *cis* dioxo complex [(hoz)₂Re(O)₂⁺] previously generated in our laboratory.⁴

Synthesis of Cationic Rhenium(V) Imido Complexes and X-ray Molecular Structure of [(salpd)Re(NMes)(PPh₃)]- $[\text{B}(\text{C}_6\text{F}_5)_4]$. Treatment of the red oxo-imido Re(VII) complexes **4–6** with excess PPh₃ results in an immediate color change to green and the formation of the cationic imido complexes **7–9** and triphenyl phosphine oxide (Scheme 2).

- (14) Neutral *cis* Re(VII) oxo-imido: (a) Gisdakis, P.; Rosch, N.; Bencze, E.; Mink, J.; Goncalves, I. S.; Kuhn, F. E. *Eur. J. Inorg. Chem.* **2001**, 981–991. (b) Hermann, W. A.; Ding, H.; Kuhn, F. E.; Scherer, W. *Organometallics* **1998**, *17*, 2751–2757. Neutral *cis* Re(VII) dioxo: (c) Wang, W.-D.; Ellern, A.; Guzei, I. A.; Espenson, J. H. *Organometallics* **2002**, *21*, 5576–5582. (d) Espenson, J. H.; Shan, X.; Wang, Y.; Huang, R.; Lahti, D. W.; Dixon, J.; Lente, G.; Ellern, A.; Guzei, I. A. *Inorg. Chem.* **2002**, *41*, 2583–2591. (e) Cai, S.; Hoffmann, D. M.; Wierda, D. A. *Organometallics* **1988**, *7*, 2069–2070. Cationic trioxo Re(VII): (f) Weighart, K.; Pomp, C.; Nuber, B.; Weiss, J. *Inorg. Chem.* **1986**, *25*, 1659–1661. Cationic *cis* dioxo Re(V): (g) Che, C.-M.; Cheng, J. Y. K.; Cheung, K.-K.; Wong, K.-Y. *J. Chem. Soc., Dalton Trans.* **1997**, 2347–2350. Neutral *trans* dioxo Re(V): (h) Paulo, A.; Reddy, K. R.; Domingos, A.; Santos, I. *Inorg. Chem.* **1998**, *37*, 6807–6813. (i) Kuckmann, T. I.; Abram, U. *Inorg. Chem.* **2004**, *43*, 7068–7074. Re(VII) dioxo alkylidene: (j) Cai, S.; Hoffman, D. M.; Wierda, D. A. *Organometallics* **1996**, *15*, 1023–1032. Oxo-imido complexes of other metals: (k) Gibson, V. C.; Graham, A. J.; Jolly, M.; Mitchell, J. P. *J. Chem. Soc., Dalton Trans.* **2003**, 4457–4465. (l) Montilla, F.; Pastor, A.; Galindo, A. *J. Organomet. Chem.* **1999**, *590*, 202–207.
- (15) A search of the Cambridge Structural Database (CSD) of rhenium diimido complexes yielded only 17 structures of rhenium(VII) complexes that did not include a third multiply bonded ligand, and out of the 17 structures only one is cationic: Cheng, J. Y. K.; Cheung, K.-K.; Chan, M. C. W.; Wong, K.-Y.; Che, C.-M. *Inorg. Chim. Acta* **1998**, *272*, 176.

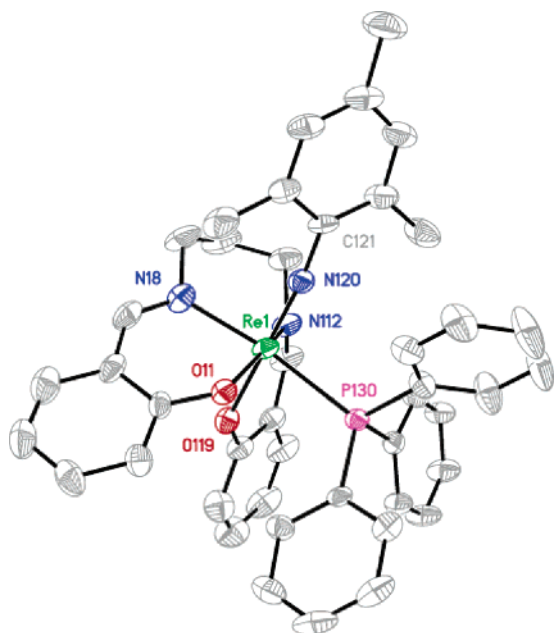


Figure 3. X-ray single-crystal structure of $[(\text{salpd})\text{Re}(\text{NMes})(\text{PPh}_3)]\text{-}[\text{B}(\text{C}_6\text{F}_5)_4]^-$, **7**. Thermal ellipsoids are 50%. Hydrogens and the anion $[\text{B}(\text{C}_6\text{F}_5)_4]^-$ have been removed for clarity. Selected bond distances (Å) and angles (deg). Re1–N120, 1.755(4); Re1–O119, 1.986(4); Re1–O11, 2.027(3); Re1–N112, 2.091(4); Re1–N18, 2.126(4); Re1–P130, 2.464(4); C121–N120–Re1, 173.1(4); N120–Re1–O119, 178.9(2); N120–Re1–O11, 100.3(2); O119–Re1–O11, 80.9(1); N120–Re1–N112, 162.6(12); O119–Re1–N112, 82.3(2); O11–Re1–N112, 162.6(2); N120–Re1–N18, 91.4(2); O119–Re1–N18, 88.4(2); O11–Re1–N18, 89.2(2); N112–Re1–N18, 85.8(1); N120–Re1–P130, 94.4(1); O119–Re1–P130, 85.8(1); O11–Re1–P130, 85.5(1); N112–Re1–P130, 97.8(1); N18–Re1–P130, 172.8(1).

Complexes **7–9** all feature *cis* (to imido) coordination of triphenyl phosphine. In all complexes, the chemical shifts of the triphenyl phosphine ligand are shifted upfield (–4 to –18 ppm) in the ^{31}P spectra relative to free triphenyl phosphine. The product of oxygen atom transfer from **4** was isolated on a preparative scale, and suitable crystals were obtained for X-ray diffraction by vapor diffusion of pentane into a concentrated methylene chloride solution of **7** at room temperature (Figure 3).

Complex **7** adopts a distorted octahedral geometry with the angles around Re ranging from 82° to 173° . The Re imido bond C121–N120–Re1 is linear ($173.1(4)^\circ$), and the Re imido bond length (1.755(4) Å) is within normal range and similar to that of the Re(VII) oxo-imido complex described above. The Re phosphorus bond length, Re–P130 (2.464(1) Å), is within normal range.¹⁶ The Re oxygen bond *cis* to the imido ligand, Re1–O11, (2.027(3) Å), is significantly lengthened (cf. to Re1–O22 in **5a**, 1.914(3) Å). The lengthening of this bond results from a repulsive interaction between the lone pairs on the alkoxide ligand and the d_{xy} electrons in this d^2 metal center. As a result, the Re oxygen bonds *cis* (2.027(3) Å) and *trans* (1.986(4) Å) to the imido ligand have similar bond lengths. This is unexpected given the strong *trans* influence of the imido ligand. Examples of filled–filled interactions between transition metal orbitals and lone pairs on ancillary ligands have been observed in other d^2 metal systems.¹⁷

(16) Chakraborty, I.; Panda, B. K.; Gangopadhyay, J.; Chakravorty, A. *Inorg. Chem.* **2005**, *44*, 1054–1060.

Stereochemistry of Oxo-Imido and Imido-Phosphine complexes. The oxo-imido complexes **4–5** and the imido complexes **7–8** feature tetradentate salen ligands. For complexes incorporating these ligands in an octahedral environment, three geometric isomers are possible (*trans*, *cis- α* , and *cis- β*) as depicted in (Scheme 3).¹⁸ In the *cis- α* isomer the phenoxide ligands of salen are *trans* to each other, while in the *cis- β* isomer both the phenoxides and imines are *cis*. In addition, two isomers of the *cis- β* structure are possible with the imido ligand *trans* to phenoxide or *trans* to the imine nitrogen. The synthesis of complexes **4–6** is stereoselective for the *cis- β* isomer (by NMR spectroscopy and X-ray crystallography). However, the current data do not rule out the possibility of rearrangement from the *cis- β* isomer to the *cis- α* isomer in solution.

Tetradentate salen-type ligands preferentially adopt a planar *trans* geometry, but this geometric isomer is precluded on an electronic basis for both types of complexes reported herein. In the oxo-imido complexes, π donation by the imido and oxo ligands is maximized through the *cis* configuration of these two ligands. In contrast, the *trans* isomer would force the multiply bonded ligands to compete for one of the d_π orbitals.

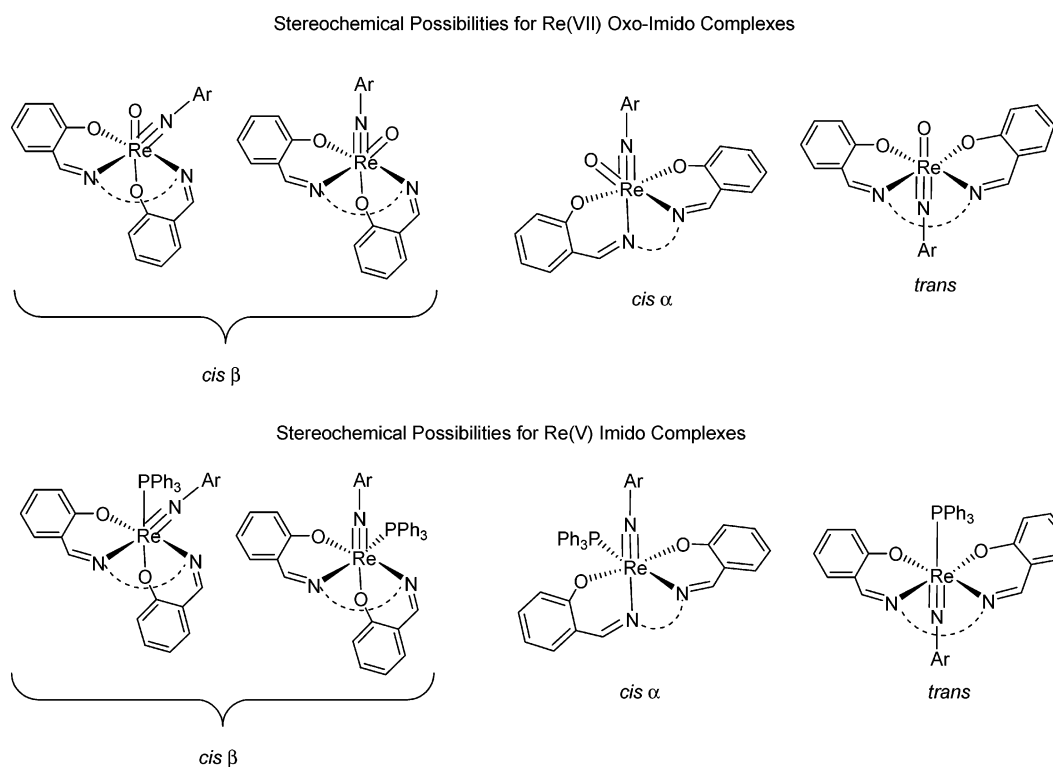
In the case of the phosphine complexes **7–8**, the π -acceptor ligand (PPh_3) favors occupying a *cis* position relative to the multiply bonded imido ligand in order to align (overlap) σ^* on PPh_3 with d_{xy}^2 . Thus the stereoselectivity realized in the synthesis of complexes **4–6** and **7–9** can be rationalized on the basis of electronics, which is minimize π competition among π donating ligands (**4–6**) and maximize overlap between d_{xy}^2 and σ^* orbitals of PPh_3 (**7–9**). Similar electronic arguments can be invoked to rationalize the preference for *cis- β* over *cis- α* . In d^0 oxo-imido complexes, the *cis- α* isomer forces the π donating phenoxide ligands *trans* to each other, and they would be competing for donation into the same d orbital. In the *cis- α* isomer of imido-phosphine complexes **7–9**, the phenoxide ligands reside in the same plane as the filled d_{xy} orbital.

From the X-ray crystal structures for **5a** and **7**, there also appears to be a stereoselective preference for the *cis- β* isomer with imido *trans* to the imine group of the saldach ligand in **5a** and *trans* to the phenoxy group in **7**. Again this stereochemical preference can be rationalized based on the need to minimize π -donor competition. In the d^0 oxo-imido complexes, a strong π donor (oxo or imido) must be *trans* to a π -donating phenoxide ligand in either of the *cis- β* geometric isomers. The isomer with the oxo ligand *trans* to phenoxide is favored because the imido ligand is a stronger π donor than the oxo ligand, and such arrangement allows the stronger π donor (imido) to maximize its π interactions. As mentioned above, an occupied molecular orbital (d_{xy}^2) occurs in the plane formed by the saldach nitrogens and one phenoxide ligand in the Re(V) imido-phosphine complexes. As a result, the strongly π -donating imido ligand is not likely to occupy the fourth position in the equatorial plane because such arrangement would result in filled–filled interactions between d_{xy}^2 and a lone pair on the imido nitrogen.

Similar arguments have been advanced for the stereochemical preferences in oxo-imido salen complexes involving other

(17) (a) Mills, R. C.; Wang, S. W. S.; Abboud, K. A.; Boncella, J. M. *Inorg. Chem.* **2001**, *40*, 5077–5082. (b) Cammeron, T. M.; Abboud, K. A.; Boncella, J. M. *Chem. Commun.* **2001**, *13*, 1224–1225. (c) Ison, E. A.; Abboud, K. A.; Boncella, J. M. *Organometallics* **2006**, *25*, 1557–1564. (18) Knight, P. D.; Scott, P. *Coord. Chem. Rev.* **2003**, *242*, 125–143.

Scheme 3



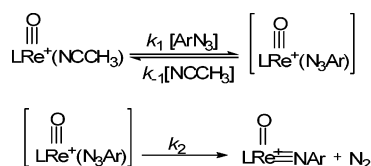
metals. For example, the *cis*- β isomer with the imido *trans* to the imine ligand has been recently observed in $[\text{Mo}(\text{O})\text{N}^t\text{Bu}]\{(\text{3,5-}^t\text{Bu}_2)_2\text{salpd}\}$, and this geometry was rationalized based on the relative π donor strengths of the oxo and imido ligands.¹⁹ However, the observation of the opposite arrangement (imido *trans* to phenoxide) in $[\text{Mo}(\text{O})(\text{N-2,6-}^i\text{Pr}_2\text{C}_6\text{H}_3)\{(\text{7-Me})_2\text{salen}\}]$ by the same authors suggests that caution should be exercised when applying qualitative “back of the envelope” electronic arguments, as other factors may be responsible for the geometric preference.

An interesting feature of the stereochemistry of the oxo-imido and imido-phosphine complexes described here is the fact that the stereochemistry changes as a result of OAT and the imido ligand switches from *trans* to imine (oxo-imido) to *trans* to phenoxide (imido-phosphine). The mechanistic implications of this change in geometry will be the subject of a future publication.

Mechanism of Oxo-imido Formation. To date two mechanisms have been postulated for the interaction of aryl azides with transition metals. Both the Bergman and Cummins laboratories have isolated azido adducts of tantalum and vanadium, respectively, and observed their thermal decomposition to imido complexes with the evolution of N_2 .⁸ Recently, we have proposed a different mechanism for the reaction of Mn(III) corrole with aryl azides in which the azide is activated thermally or photochemically to afford a nitrene intermediate that is subsequently trapped by the manganese corrole.⁹ Additionally ortho substituents on the aryl azide are necessary, and the reaction exhibits complex dependencies on Mn with a zeroth-order dependence for a significant portion of the reaction.⁹

In contrast, the formation of complexes **4–6** does not require thermal or photochemical activation, and the reaction is not

Scheme 4



$$\frac{d[\text{LRe}^{\text{VII}}(\text{O})(\text{NR})^+]}{dt} = \frac{k_1 k_2 [\text{LRe}(\text{O})(\text{NCCH}_3)^+][\text{ArN}_3]}{k_{-1}[\text{NCCH}_3] + k_1[\text{ArN}_3]} \quad (1)$$

restricted to aryl azides containing ortho substituents. The reaction reported herein is quite versatile and proceeds with both electron rich and electron deficient azides (Scheme 1). In light of these observations it is apparent that the formation of complexes **4–6** does not proceed via nitrene capture. The kinetics of the formation of **5d** from **2** and *p*- CF_3 phenyl azide were studied in detail by monitoring product formation in the ^{19}F spectra at ambient conditions. As shown in Figure 4, the reaction exhibits first-order dependencies on complex **2** (time profile) and *p*- CF_3 phenyl azide (inset).

When **2** is treated with 1 equiv of *p*- CF_3 phenyl azide at -80°C in CD_2Cl_2 , in addition to signals for the organic azide (-62.2 ppm) and **5d** (-63.5 ppm), an additional peak is observed at -63.8 ppm in the ^{19}F spectrum in the integral ratios of 13:6:1, respectively. When the temperature was raised to -30°C , the azide signal (-62.2 ppm) and the signal at -63.8 ppm converted slowly to **5d**. These results suggest that the reaction of complexes **1–3** with aryl azides proceeds through a mechanism analogous to that proposed by Bergman for the reaction of organic azides with $\text{Cp}_2\text{TaMe}(\text{PMe}_3)$; i.e., an organoazido adduct of rhenium is initially formed followed by its decomposition to give the Re(VII) oxo imido complex and N_2 . A consensus mechanism is depicted in Scheme 4 along with

(19) Ramnauth, R.; Al-Juaid, S.; Motevalli, M.; Parkin, B. C.; Sullivan, A. C. *Inorg. Chem.* **2004**, *43*, 4072–4079.

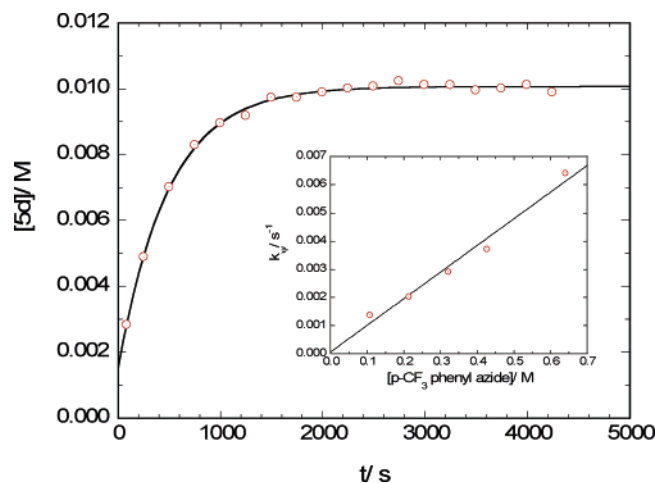


Figure 4. A typical time profile for the reaction of **2** with *p*-CF₃ phenyl azide. The signal for the product **5d** at δ -63.5 was monitored by ¹⁹F NMR spectroscopy. Conditions: 20.8 mM **2**, 8.0 M CH₃CN, 0.10–0.65 M *p*-CF₃ phenyl azide in C₆D₆ at 298 K. The data are shown for 0.20 M *p*-CF₃ phenyl azide. The fit is to single-exponential first-order equation $[5d]_t = [2][1 - \exp(-k_{\text{obs}}t)]$. Inset: Dependence on *p*-CF₃ phenyl azide. Linear fit gives a second-order rate constant $(9.4 \pm 0.8) \times 10^{-3} \text{ M}^{-1} \text{ s}^{-1}$ ($R^2 = 0.977$). According to eq 1, $K_1k_2 = \text{slope} \times [\text{NCCH}_3]$; $K_1k_2 = 0.075 \pm 0.006 \text{ s}^{-1}$.

its corresponding rate law in eq 1, assuming a prior equilibrium for the formation of the organoazido adduct/intermediate.

The observed reactivity is consistent with the fact that Re(V) complexes used here are easier to oxidize than Mn(III) and therefore do not require thermal or photochemical activation of the azide. Such reactivity is consistent with the periodic trend that second and third row transition metals stabilize higher oxidation states and thus tend to be more reducing than their first row counterparts.

Oxygen Atom Transfer Reactions of Rhenium(VII) Oxo-Imido Complexes. The reactions of **5** with PPh₃ were investigated under pseudo-first-order conditions using stopped-flow spectroscopy. The progress of the reaction was monitored at 500 nm, where the cationic rhenium(VII) oxo-imido complex [(saldach)Re(NAr)(O)][B(C₆F₅)₄], **5**, absorbs but the rhenium(V) imido product [(saldach)Re(NAr)(OPPh₃)][B(C₆F₅)₄], **10**, does not. The disappearance of **5** monitored at 500 nm displayed clean first-order kinetics in Re (Figure S1). A plot of k_{obs} versus [PPh₃] revealed saturation kinetics for the dependence on PPh₃ (Figure 5). The plateau value was not affected by the addition of excess triphenyl phosphine oxide. Furthermore, when the reaction of **5** with triphenyl phosphine was monitored by ³¹P NMR spectroscopy a triphenyl phosphine oxide adduct (δ 41.0), **10**, was observed prior to the formation of the phosphine adduct **8** (isolated product). These results suggest that the reduction of **5** occurs at a different rate than the formation of **8**; i.e., the substitution of triphenyl phosphine oxide by free triphenyl phosphine is slower than the reduction of **5** to the rhenium(V) imido phosphine oxide adduct, [(saldach)Re(NAr)(OPPh₃)⁺] (**10**).

Metal oxo complexes are known to oxidize organic phosphines, and the mechanism for this reaction has been extensively discussed and is generally believed to proceed through a direct attack of the phosphine on the metal oxo.²⁰ Usually these reactions exhibit bimolecular kinetics, and saturation kinetics is not observed.²¹ The observed kinetic saturation in [phosphine]

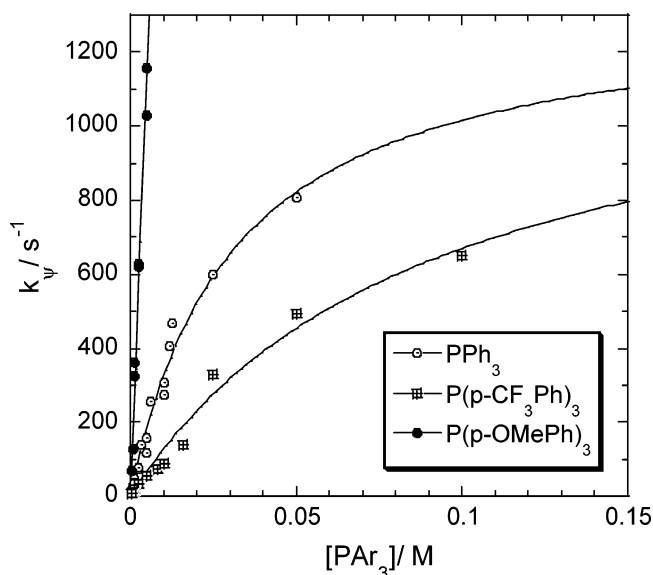


Figure 5. PAR₃ dependences for the reaction of [(saldach)Re(O)(NMes)-[B(C₆F₅)₄], **5a**, with PAR₃ (Ar = phenyl, *p*-OMe phenyl, or *p*-CF₃ phenyl) monitored at 500 nm. Conditions: [**5a**] = 50 μM and [PPh₃] = 0.625–50.0 mM, [P(*p*-CF₃Ph)₃] = 0.313–100 mM, or [P(*p*-OMePh)₃] = 0.313–5.0 mM in CH₃CN at 298 K. The fits are to eq 2 for PPh₃ and P(*p*-CF₃Ph)₃ and to a linear equation for P(*p*-OMePh)₃.

for our complexes suggests that mechanisms involving rate-determining attack of PPh₃ on the metal oxo can be ruled out. The data presented here appear to be in agreement with three kinetically indistinguishable schemes. The oxo-imido complex reacts with PPh₃ to form, in a prior equilibrium step, an adduct preceding OAT (Scheme 5A, eq 2). In this adduct initial attack of the PPh₃ ligand results in an intermediate that resembles [Re^(VII)=O---PPh₃] more than [Re^(V)←O=PPh₃]. By analogy to Taube's inner-sphere electron transfer, the intermediate in Scheme 5A is the precursor complex and the product the successor complex. Although intermediates of this form have not been directly isolated, similar intermediates have been proposed in the reaction of bis(arylimido)oxorhenium(VII) complexes,²² oxorhenium(V) complexes,²³ and arylimido ruthenium(IV) complexes²⁴ with organic phosphines. Alternatively, the oxo-imido complex isomerizes to an active steady-state intermediate where the stereochemistry of the imido ligand switches from *trans* to imine to *trans* to phenoxy (most likely via the *cis*- α isomer). The resulting intermediate then subsequently reacts with PPh₃ (Scheme 5B, eq 3). Another mechanism along the same lines is separation of the ion pair [LRe^{VII}(O)(NAr)⁺][B(C₆F₅)₄⁻] (Scheme 5C, eq 4). This last pathway is unlikely because the reactions were carried out in a polar medium (acetonitrile) where the ions are expected to be well separated.

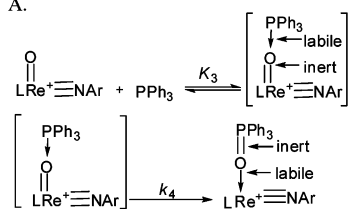
In order to interrogate these mechanisms further, we compared the kinetic behavior of three different triarylphosphines, PAR₃ (Ar = phenyl, *p*-CF₃ phenyl, or *p*-OMe phenyl). Changing the phosphine substrate would have an effect on the saturation value in Scheme 5A, as the saturation value is governed by k_4 .

- (21) (a) Pietsch, M. A.; Hall, M. B. *Inorg. Chem.* **1996**, *35*, 1273–1278. (b) Tucci, G. C.; Donahue, J. P.; Holm, R. H. *Inorg. Chem.* **1998**, *37*, 1602–1608.
 (22) Wang, W.-D.; Guzei, I. A.; Espenson, J. H. *Organometallics* **2001**, *20*, 148–156.
 (23) Li, M.; Ellern, A.; Espenson, J. H. *J. Am. Chem. Soc.* **2005**, *127*, 10436–10447.
 (24) Leung, W.-H.; Hun, T. S. M.; Hou, H.-W.; Wong, K.-Y. *J. Chem. Soc., Dalton Trans.* **1997**, 237–243.

(20) Seymore, S. B.; Brown, S. N. *Inorg. Chem.* **2000**, *39*, 325–332.

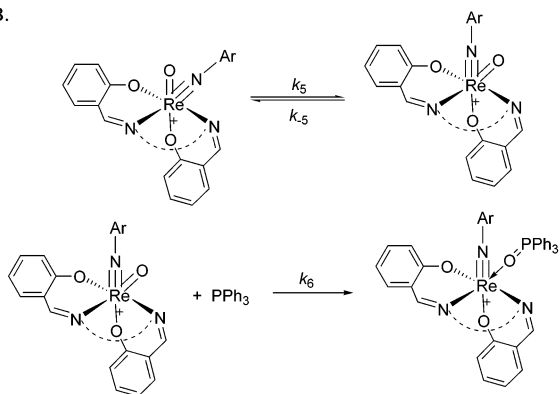
Scheme 5

A.



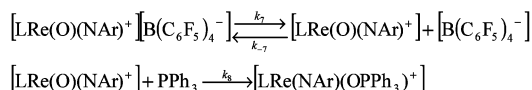
$$-\frac{d[\text{LRe}(\text{O})(\text{NAr})^+]}{dt} = \frac{k_4[\text{LRe}(\text{O})(\text{NAr})^+][\text{PPh}_3]}{1/K_3 + [\text{PPh}_3]} \quad (2)$$

B.



$$-\frac{d[\text{LRe}(\text{O})(\text{NAr})^+]}{dt} = \frac{k_5[\text{LRe}(\text{O})(\text{NAr})^+][\text{PPh}_3]}{k_{-5}/k_6 + [\text{PPh}_3]} \quad (3)$$

C.



$$-\frac{d[\text{LRe}(\text{O})(\text{NAr})^+]}{dt} = \frac{k_7[\text{LRe}(\text{O})(\text{NAr})^+][\text{PPh}_3]}{k_{-7}/k_8[\text{B}(\text{C}_6\text{F}_5)_4]^- + [\text{PPh}_3]} \quad (4)$$

However, changing the phosphine would not affect the saturation values k_5 and k_7 according to Schemes 5B and C. Furthermore, the observation of saturation kinetics permits the separation of the “apparent” second-order rate constant to its components, an equilibrium constant for formation of the phosphine adduct and a first-order rate constant for the redox atom transfer reaction in which the Re=O bond is cleaved and the P=O bond is formed.

Plots of k_p versus $[\text{PAR}_3]$ for all three phosphine substrates are shown in Figure 5. The kinetic data clearly favor the mechanism presented in Scheme 5A because the plateau values are substrate specific. $\text{P}(p\text{-OMePh})_3$ does not exhibit saturation within the measurement limits of stopped-flow. Nevertheless, all three phosphine substrates give second-order rate constants that follow a Hammett correlation with a negative reaction constant, $\rho = -0.6 \pm 0.1$ (Figure S2).

A significant structural change occurs along the oxygen atom transfer reaction pathway from the Re(VII) oxo-imido complex to the Re(V) imido phosphine complex. The imido ligand in complexes 4–6 is *trans* to the imine group of the saldach ligand and becomes *trans* to the phenoxide group of the saldach ligand in the isolated products 7–9. Previously, in our labs similar

structural changes were observed to accompany OAT of the Re(V) oxazoline complex 3 to the Re(VII) dioxo complex $[(\text{hoz})_2\text{Re}(\text{O})_2]^+$ (11).⁴ The Re(V) complex, 3, begins with a solvent molecule (water or acetonitrile) in a *trans* configuration with respect to the oxo ligand, and as a result of oxygen atom transfer the two oxo ligands in the Re(VII) dioxo complex, 11, are arranged *cis*. These structural changes were proposed to occur as a result of substitution of the solvent molecule in 3, with an oxo donor substrate that enters *cis* to the oxo ligand. As a result of the *cis* entry of the oxo donor substrate, the oxazoline ligand in 3 undergoes a geometrical change to accommodate the incoming oxo donor ligand and facilitate OAT. Similar geometric changes associated with ligand substitution reactions have also been suggested for dithiolate Re(V) complexes.²⁵ Thus a reasonable mechanism for substitution of triphenyl phosphine oxide via a solvent adduct is depicted in Scheme 6, which accounts for the change in imido ligand from *trans* to imine to *trans* to phenoxide. The details of the mechanism of substitution of OPPh_3 and the geometric changes associated with this substitution, however, are beyond the scope of this article.

Comparison of Oxygen Atom Transfer (OAT) Reactivity.

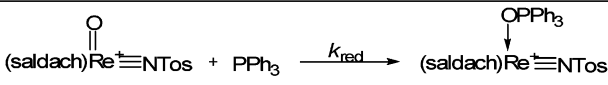
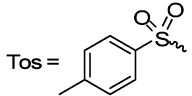
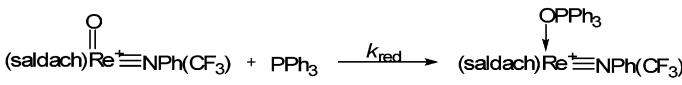
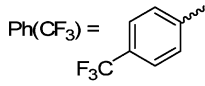
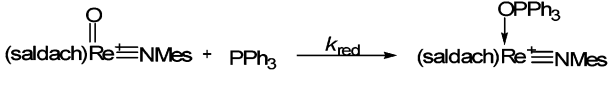
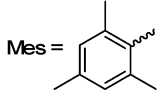
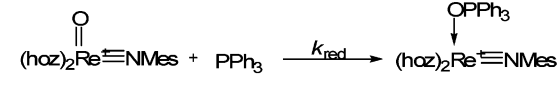
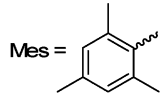

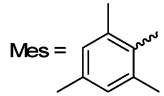
The synthesis of oxo-imido complexes 4–6 allows us to compare directly the chemistry of these complexes with the cationic *cis* dioxo complex $[(\text{hoz})_2\text{Re}(\text{O})_2]^+$ (11). This complex has been shown to be an effective catalyst for the reduction of perchlorate at room temperature, and it has been demonstrated that oxygen atom transfer is the operational mechanism during this catalysis.⁴ Unlike, complexes 4–6, which are stable to air and moisture and isolable on a preparative scale, 11 could only be prepared in situ and could not be isolated. In addition, in complexes 4–6, the sterics and electronics of the substituents on the imido ligands can be varied in order to tune their reactivity.

First, we examined the effect changing the electronics of the imido substituent has on the rate of OAT to PPh_3 by measuring the rates for a series of complexes at 500 nm in CH_3CN by stopped-flow spectroscopy. All complexes displayed first-order dependencies on Re and saturation kinetics on PPh_3 . The rate and equilibrium constants in accordance with Scheme 5A and eq 2 are summarized in Table 1. From Table 1, two features of this system are readily apparent. The oxazoline complex 6a is somewhat less reactive (ca. 0.25 times) than the corresponding saldach complex 5a (second-order rate constants 1.1×10^4 vs $4.3 \times 10^4 \text{ M}^{-1} \text{ s}^{-1}$). Second, the rate of oxygen atom transfer reactions is influenced greatly by the electronics of the ancillary imido ligand such that the rate increases dramatically as the imido ligand becomes more electron-deficient. The tosyl substituted imido 5e reacts faster than the stopped-flow dead time, and the *p*- CF_3 phenyl substituted oxo imido complex 5d is approximately 13 times more reactive than the corresponding mesityl imido complex 5a. Thus a general order of reactivity for the imido ligand substituent is $\text{Tos} > p\text{-CF}_3 \text{ phenyl} > \text{Mes}$. This trend is indicative of electrophilic oxo transfer from the oxo-imido complexes to the substrate.

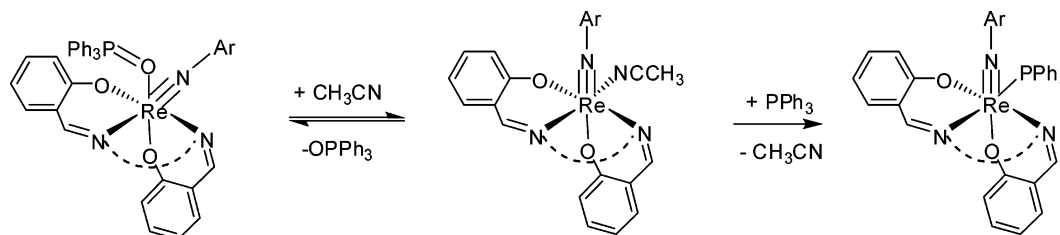
In order to compare the rates of OAT directly with the *cis* dioxo complex, we examined the rates of OAT to other substrates because OAT to PPh_3 from $[(\text{hoz})_2\text{Re}(\text{O})_2]^+$ (11) was

(25) Lahti, D. W.; Espenson, J. H. *J. Am. Chem. Soc.* **2001**, *123*, 6014–6024.

Table 1. Comparison of Rate and Equilibrium Constants for the Reaction of Select Oxo-Imido Complexes with PPh₃^a

Reaction	Symbol	Value
 	k_{red}	N.A. ^b
 	K_3 k_4	$441 \pm 18 \text{ M}^{-1}$ $1290 \pm 25 \text{ s}^{-1}$
 	K_3 k_4	$32 \pm 5 \text{ M}^{-1}$ $1331 \pm 129 \text{ s}^{-1}$
 	K_3 k_4	$45 \pm 3 \text{ M}^{-1}$ $236 \pm 4 \text{ s}^{-1}$
 	$k_{\text{red}} = K_3 k_4$	$1.06 \pm 0.07 \times 10^4 \text{ M}^{-1} \text{ s}^{-1}$

^a Values are obtained from a nonlinear fit to the equation $(-d[\text{LRe}(\text{O})(\text{NAr})^+]/dt) = (k_4[\text{LRe}(\text{O})(\text{NAr})^+][\text{PPh}_3])/(1/K_3 + [\text{PPh}_3])$. ^b This rate was not observed because it is faster than the dead time of the stopped-flow analyzer (2 ms).

Scheme 6

too fast to measure by stopped-flow. The second-order rate constants for these reactions are gathered in Table 2.

As expected for electrophilic oxygen atom transfer, aryl sulfides are less reactive than aryl thiols,²⁶ which are less reactive than PPh₃ (entries 3–5). The rate of OAT from [(hoz)₂Re(O)₂]⁺ has been determined and can be directly compared with our isoelectronic cationic rhenium(VII) oxo-imido complexes. From Table 2, a dramatic effect on the rates of OAT is seen as the imido substituent is varied. While the *p*-CF₃ phenyl substituted oxo-imido complex is 10⁵ times less reactive than the dioxo, changing the imido substituent to the more electron-withdrawing tosyl group leads to a 1000-fold improvement in the rate of OAT (entries 2 and 3), and this tosyl imido complex is now only 300 times less reactive than the dioxo complex. This is a clear demonstration of the tunability of these oxo-imido complexes toward atom transfer reactions.

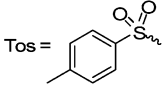
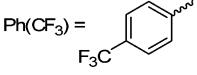
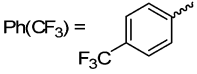
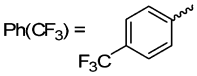
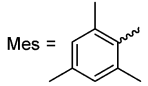
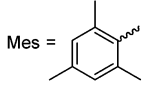
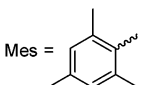
(26) For an example of thiols oxidation to disulfides with rhenium oxo, see: Abu-Omar, M. M.; Khan, S. I. *Inorg. Chem.* **1998**, *37*, 4979–4985.

The higher reactivity of the dioxo complex in comparison to the electron-withdrawing tosyl imido complex (entry 1 vs 2) is a direct demonstration of the enhanced electron donation exerted by the imido ligand, which stabilizes rhenium(VII) more effectively than a terminal oxo.

Summary and Conclusions

The development of methods for the synthesis of transition metal imido complexes is of interest because of their implication in catalysis, particularly, in [NR] group transfer chemistry. We have demonstrated a facile method for the synthesis of cationic Re(VII) *cis* oxo-imido complexes from aryl azides under ambient conditions without the need for thermal or photochemical activation of the organic azide. Mechanistic interrogation suggests the reactions of Re(V) with aryl azides proceed through an azido adduct similar to the group 5 complexes of Bergman and Cummins.⁸ The only byproduct from the organic azide is N₂; thus the method presented in this paper does not require

Table 2. Second-Order Rate Constants for the Following OAT Reaction: $\text{LRe}^{\text{VII}}(\text{O})(\text{E})^+ + \text{Y} \rightarrow \text{LRe}^{\text{V}}(\text{E})^+ + \text{YO}$; E = O or NAr, and L = hoz or Saldach^a

Entry	Substrate (Y)	Complex	k_{red} (298K) / L mol ⁻¹ s ⁻¹
1	PhSMe	$[(\text{hoz})_2\text{Re}(\text{O})_2]^+$	110 ± 8^b
2	PhSMe	$[(\text{saldach})\text{Re}(\text{O})(\text{NTos})]^+$	0.31 ± 0.05
			
3	PhSMe	$[(\text{saldach})\text{Re}(\text{O})(\text{NPh}(\text{CF}_3))]^+$	$2.5 \pm 0.6 \times 10^4$
			
4	PhSH	$[(\text{saldach})\text{Re}(\text{O})(\text{NPh}(\text{CF}_3))]^+$	0.29 ± 0.03
			
5	PPh ₃	$[(\text{saldach})\text{Re}(\text{O})(\text{NPh}(\text{CF}_3))]^+$	$5.7 \pm 0.3 \times 10^5$
			
6	PPh ₃	$[(\text{saldach})\text{Re}(\text{O})(\text{NMes})]^+$	$4.3 \pm 0.8 \times 10^4$
			
7	P(<i>p</i> -CF ₃ Ph) ₃	$[(\text{saldach})\text{Re}(\text{O})(\text{NMes})]^+$	$1.4 \pm 0.5 \times 10^4$
			
8	P(<i>p</i> -OMePh) ₃	$[(\text{saldach})\text{Re}(\text{O})(\text{NMes})]^+$	$2.27 \pm 0.07 \times 10^5^c$
			

^a Apparent second-order rate constant = K_3k_4 obtained from a nonlinear fit to the equation $(-d[\text{LRe}(\text{O})(\text{NAr})^+])/dt = (k_4[\text{LRe}(\text{O})(\text{NAr})^+][\text{Y}])/(1/K_3 + [\text{Y}])$. ^b Obtained from ref 4. ^c Obtained from a linear fit because the data for this substrate did not show saturation within the stopped-flow time scale.

tedious chromatography to separate organic byproducts. Furthermore, the synthesis of imido complexes from aryl azides in high yield has allowed us to characterize crystallographically the first example of a cationic Re(VII) oxo-imido complex.

Unlike the previously reported cationic Re(VII) dioxo complexes, which have been observed in situ but not isolated,^{3,4} the cationic oxo-imido complexes are obtained on a preparative scale. In addition, the chemistry of these complexes toward oxygen atom transfer (OAT) reactions can be compared directly with the cationic dioxo complex $[(\text{hoz})_2\text{Re}(\text{O})_2]^+$, which was previously shown to be an effective OAT catalyst.⁴ Rates of OAT reactions are significantly affected by the electronics of the imido ancillary ligand with electron-withdrawing imidos

being most effective. For example, the tosyl substituted imido complex is more reactive (ca. 10^3 times) than the *p*-CF₃ phenyl imido complex, which in turn is an order of magnitude more reactive than the mesityl imido complex. However, the most reactive tosyl imido complex remains 300 times slower in OAT reactions than the dioxo analogue. Consistent with the observed trend is the rate sensitivity toward the oxygen acceptor. Aryl phosphines are more reactive than thiophenol (PhSH), which is more reactive than thioanisole (PhSMe). Also within the family of aryl phosphines, electron-donating substituents are more reactive than electron-withdrawing substituents affording a negative Hammett reaction constant. These reactivity trends confirm electrophilic oxygen atom transfer from Re(VII) oxo-

imido complexes. The ability to tune the reactivity of cationic rhenium(VII) imido complexes should have a bearing on the intelligent design of catalysts for [NR] group transfer from organic azides, an appealing methodology because its only waste is molecular nitrogen (N₂). Work is currently being undertaken in our laboratory toward the development of suitable complexes for such group transfer catalysis.

Experimental Section

Materials and Methods. Reactions were performed in a nitrogen-filled glovebox or open to the environment as stated. Solvents were degassed and purified with a solvent purification system (Anhydrous Engineering INC.) prior to use. Thiols, sulfides, and aryl phosphines were purchased from Aldrich and used as received. The cationic rhenium mono-oxo salen complexes, [(salpd)Re(O)(Solv)][B(C₆F₅)₄] (**1**) and [(saldach)Re(O)(Solv)][B(C₆F₅)₄] (**2**), and the mono-oxo oxazoline complex [(hoz)₂Re(O)(Solv)][B(C₆F₅)₄] (**3**) were synthesized according to published procedures.^{4,12} NMR spectra were recorded on Varian Inova300 instruments. Mass spectrometry was performed by the Purdue University Campus Wide Mass Spectrometry Center. UV-vis spectra were recorded on a Shimadzu UV-2501 spectrophotometer. Stopped-flow kinetics was collected on an Applied Photophysics SX.18MV stopped-flow reaction analyzer. Data fitting was done using KaleidaGraph 3.0 software.

Synthesis of Cationic Re(VII) Oxo-Imido Complexes. [(salpd)Re(O)(NMe₃)] [B(C₆F₅)₄] (**4**). **(Typical Procedure).** [(salpd)Re(O)(Solv)][B(C₆F₅)₄] (**1**, 0.200 g, 0.167 mmol) was dissolved in CH₂Cl₂. To this solution was added 2,4,6-trimethyl phenyl azide (0.027 g, 0.167 mmol). The solution changed color from green to red and was stirred overnight. The solvent was removed under a vacuum, and the residue dissolved in a minimal amount of CH₂Cl₂. Pentane was added until a red powder precipitated. The red powder was washed several times with pentane to yield **4** in 66% (0.231 g) yield. ¹H NMR (300 MHz, CD₂Cl₂): δ 8.45 (s, 1H, C=N-H), 8.34 (s, 1H, C=N-H), 7.79–7.73 (m, 1H, overlapping aromatic), 7.60–7.52 (m, 2H, overlapping aromatic), 7.35–7.33 (m, 1H, overlapping aromatic), 7.24–7.19 (m, 1H, overlapping aromatic), 7.14–7.12 (d, 1H, J = 8.20 Hz, aromatic CH), 7.08 (s, 2H, overlapping aromatic), 6.96–6.91 (m, 1H, overlapping aromatic), 6.71–6.68 (d, 1H, J = 8.79, aromatic CH), 4.66–4.51 (m, 3H, salpd CH₂), 4.10–4.04 (m, 1H, salpd CH₂), 3.01 (s, 3H, *p*-CH₃), 2.64 (s, 6H, CH₃), 2.15–2.13 (m, 2H, salpd CH₂). ¹³C NMR (300 MHz, CD₃CN): δ 168.5, 166.6, 163.4, 158.9, 154.5, 151.4, 149.7, 148.7, 146.5, 139.7, 137.1, 134.7, 133.7, 128.3, 123.8, 121.5, 121.0, 120.2, 66.9, 59.7, 31.0, 21.3, 17.8. Elemental Analysis Calcd for C₅₀H₂₇BF₂₀N₃O₃Re: C, 46.4; H, 2.10; N, 3.25. Found: C, 46.5; H, 2.47; N, 2.86.

[(saldach)Re(O)(NMe₃)] [B(C₆F₅)₄] (**5a**). [(saldach)Re(O)(Solv)][B(C₆F₅)₄] (**2**, 0.100 g, 0.080 mmol) was dissolved in CH₂Cl₂. To this solution was added 2,4,6-trimethyl phenyl azide (0.0158 g, 0.099 mmol). The solution changed color from green to red and was stirred overnight. The solvent was removed under a vacuum, and the residue was dissolved in a minimal amount of CH₂Cl₂. Pentane was added until a red powder precipitated. The red powder was washed several times with pentane to yield **5a** in 66% (0.0737 g) yield. ¹H NMR (300 MHz, CD₂Cl₂): δ 8.77 (s, 1H, C=N-H), 8.75 (s, 1H, C=N-H), 7.85–7.81 (2H, overlapping aromatic), 7.57–7.51 (2H, overlapping aromatic), 7.32–7.26 (2H, overlapping aromatic), 7.09–6.99 (2H, overlapping aromatic), 6.91–6.83 (2H, overlapping aromatic), 4.40–4.33 (m, 1H, saldach CH₂), 3.13–3.25 (m, 1H, saldach CH₂), 2.77 (s, 3H, *p*-CH₃), 2.68 (s, 6H, CH₃), 2.58–2.47 (m, 2H, saldach CH₂), 2.05 (m, 2H, saldach CH₂), 1.87–1.78 (m, 2H, saldach CH₂), 1.60–1.40 (m, 2H, saldach CH₂). ¹³C NMR (300 MHz, CD₃CN): δ 164.7, 161.8, 150.1, 145.4, 143.2, 139.2, 137.2, 135.8, 133.5, 127.7, 124.1, 120.5, 120.2, 79.8, 73.7, 31.5, 29.8, 25.0, 24.3, 21.1, 17.8. Elemental Analysis Calcd for C₅₃H₃₁BF₂₀N₃O₃Re: C, 47.7; H, 2.34; N, 3.15. Found: C, 47.7; H, 2.34; N, 2.92.

[(saldach)Re(O)(NAr)][B(C₆F₅)₄], Ar = *p*-Ome Phenyl (**5b**). [(saldach)Re(O)(Solv)][B(C₆F₅)₄] (**2**, 0.100 g, 0.080 mmol) in CH₂-Cl₂ was added to *p*-Ome phenyl azide (0.0125 g, 0.084 mmol). **5b** was obtained in 63% (0.084 g) yield. ¹H NMR (200 MHz, CD₃CN): δ 8.58 (s, 1H, C=N-H), 8.51 (s, 1H, C=N-H), 7.84–7.82 (1H, overlapping aromatic), 7.77–7.69 (2H, overlapping aromatic), 7.50–7.47 (1H, overlapping aromatic), 7.30–7.27 (2H, overlapping aromatic), 7.05–6.98 (2H, overlapping aromatic), 6.90–6.86 (2H, overlapping aromatic), 6.76–6.72 (2H, overlapping aromatic), 4.31 (m, 1H, saldach CH₂), 4.02 (s, 3H, *p*-CH₃), 3.15 (m, 1H, saldach CH₂), 3.69 (m, 1H, saldach CH₂), 2.51–2.48 (m, 1H, saldach CH₂), 2.17–2.14 (m, 3H, saldach CH₂), 1.65–1.44 (m, 3H, saldach CH₂). ¹³C NMR (200 MHz, CD₃CN): δ 167.7, 164.5, 162.0, 157.3, 150.0, 147.4, 145.2, 139.2, 138.1, 137.1, 135.9, 135.3, 133.2, 125.7, 123.5, 120.3, 118.8, 117.2, 114.3, 79.2, 73.5, 56.9, 31.2, 29.4, 24.8, 24.1. Elemental Analysis Calcd for C₅₁H₂₇BF₂₀N₃O₄Re: C, 46.3; H, 2.06; N, 3.18. Found: C, 46.6; H, 2.16; N, 3.03.

[(saldach)Re(O)(NAr)][B(C₆F₅)₄], Ar = *p*-Me Phenyl (**5c**). [(saldach)Re(O)(Solv)][B(C₆F₅)₄] (**2**, 0.101 g, 0.080 mmol) in CH₂-Cl₂ was added to *p*-Me phenyl azide (10.5 μL, 0.084 mmol). **5c** was obtained in 81% (0.089 g) yield. ¹H NMR (300 MHz, CD₂Cl₂): δ 8.60 (s, 1H, C=N-H), 8.55 (s, 1H, C=N-H), 7.88–7.83 (1H, overlapping aromatic), 7.79–7.72 (2H, overlapping aromatic), 7.49–7.44 (1H, overlapping aromatic), 7.34–7.27 (4H, overlapping aromatic), 7.05–6.99 (2H, overlapping aromatic), 6.65–6.62 (d, 2H, J = 8.20 Hz, aromatic CH), 4.34–4.28 (m, 1H, saldach CH₂), 3.18–3.12 (m, 1H, saldach CH₂), 2.89 (s, 3H, *p*-CH₃), 2.77–2.69 (m, 2H, saldach CH₂), 2.52–2.45 (m, 2H, saldach CH₂), 1.91–1.76 (m, 2H, saldach CH₂), 1.57–1.44 (m, 2H, saldach CH₂). ¹³C NMR (300 MHz, CD₃CN): 165.4, 162.8, 150.7, 145.9, 140.3, 136.5, 134.0, 132.0, 129.5, 124.6, 121.3, 120.8, 119.6, 80.1, 74.1, 32.0, 30.2, 25.5, 24.8, 22.2. Elemental Analysis Calcd for C₅₁H₂₇BF₂₀N₃O₃Re: C, 46.9; H, 2.08; N, 3.22. Found: C, 47.2; H, 2.40; N, 2.92.

[(saldach)Re(O)(NAr)][B(C₆F₅)₄], Ar = *p*-CF₃ Phenyl (**5d**). [(saldach)Re(O)(Solv)][B(C₆F₅)₄] (**2**, 0.102 g, 0.085 mmol) in CH₂-Cl₂ was added to *p*-CF₃ phenyl azide (13.0 μL, 0.092 mmol). **5d** was obtained in 69% (0.079 g) yield. ¹H NMR (300 MHz, CD₂Cl₂): δ 8.65 (s, 2H, C=N-H), 7.93–7.88, (1H, overlapping aromatic), 7.80–7.74 (4H, overlapping aromatic), 7.50–7.47 (1H, overlapping aromatic), 7.39–7.29 (2H, overlapping aromatic), 7.06–7.00 (2H, overlapping aromatic), 6.86–6.83 (d, 2H, J = 8.20 Hz, aromatic CH), 4.36 (m, 1H, saldach CH₂), 3.18 (m, 1H, saldach CH₂), 2.74–2.70 (m, 1H, saldach CH₂), 2.55 (m, 1H, saldach CH₂), 2.17–2.13 (m, 3H, saldach CH₂), 1.63–1.54 (m, 3H, saldach CH₂). ¹⁹F NMR (300 MHz, CD₂-Cl₂): δ -63.7 (s, 3F, *p*-CF₃), -133.1 (s, 8F, B(C₆F₅)₄⁻), -163.5 (t, 4F, J = 19.9 Hz, B(C₆F₅)₄⁻), -167.3 (s, 8F, B(C₆F₅)₄⁻). Elemental Analysis Calcd for C₅₁H₂₃BF₂₃N₃O₃Re: C, 45.0; H, 1.78; N, 3.09. Found: C, 44.7; H, 2.05; N, 2.90.

[(saldach)Re(O)(NAr)][B(C₆F₅)₄], Ar = *p*-Tolyl Sulfonyl (**5e**). [(saldach)Re(O)(Solv)][B(C₆F₅)₄] (**2**, 0.0500 g, 0.042 mmol) was dissolved in CH₂Cl₂. To this solution was added *p*-tolyl sulfonyl (tosyl) azide (6.5 μL, 0.042 mmol). The solution changed color from green to red and was stirred overnight. The solvent was removed under a vacuum, and the residue was dissolved in a minimal amount of CH₂-Cl₂. Pentane was added until a light red/brown powder precipitated. The powder was quickly washed several times with pentane to yield **5e** in 82% (0.0472 g) yield. Complex **5e** is very unstable and decomposes quickly in both the solid state and in solution. As a result complex **5e** could only be isolated in low purity. ¹H NMR (300 MHz, CD₂Cl₂): δ 8.97 (s, 1H, C=N-H), 8.60 (s, 1H, C=N-H), 8.01–7.96 (m, 1H, aromatic), 7.78–7.73 (m, 3H, overlapping aromatic), 7.59–7.56 (d, 2H, J = 8.8 Hz, aromatic CH), 7.45–7.31 (m, 5H, overlapping aromatic), 6.80–6.77 (d, 1H, J = 8.20 Hz, aromatic CH), 4.38–4.30 (m, 1H, saldach CH₂), 3.43 (s, 3H, *p*-CH₃), 3.11–3.03 (m, 1H, saldach CH₂), 2.64–2.62 (m, 2H, saldach CH₂), 2.43 (s, 2H, CH₂), 2.30–2.14 (m, 2H, saldach CH₂), 1.88–1.75 (m, 2H, saldach CH₂). Elemental

Analysis Calcd for $C_{53}H_{31}BCl_4F_{20}N_3O_5ReS$ (with two molecules of CH_2Cl_2): C, 41.32; H, 2.03; N, 2.73. Found: C, 40.64; H, 2.60; N, 2.39.

[(hoz)₂Re(O)(NMes)][B(C₆F₅)₄] (6a). A round-bottom flask equipped with a magnetic stir bar was charged with [(hoz)₂Re(O)(Solv)][B(C₆F₅)₄], **3**, (0.182 g, 0.146 mmol) dissolved in CH_2Cl_2 . To this solution was added 2,4,6-trimethyl phenyl azide (0.0235 g, 0.147 mmol). The reaction flask was capped, and the solution was stirred for 2 h as it changed color from green to deep red. The solution was concentrated under a vacuum to an approximate volume of 5 mL. With stirring 100 mL of pentane was added. Microcrystalline red/brown solid precipitated. The precipitate was isolated by filtration, washed with pentane, and dried under a vacuum to give **6a** in 27% (0.031 g) yield. ¹H NMR (300 MHz, CD₃NO₂): δ 7.82 (d, 1H, *J* = 8.2 Hz), 7.78 (d, 1H, *J* = 8.2 Hz), 7.41 (s, 1H, imido aromatic), 7.32–7.28 (2H, overlapping hoz aromatic), 7.26 (s, 1H, imido aromatic), 6.91 (t, 1H, *J* = 8.2 Hz), 6.80 (t, 1H, *J* = 8.2 Hz), 6.33 (d, 1H, *J* = 8.2 Hz), 6.20 (d, 1H, *J* = 8.2 Hz), 5.01–4.80 (m, 5H, overlapping hoz CH₂), 4.54–4.45 (m, 2H, overlapping hoz CH₂), 4.29–4.13 (m, 1H, hoz CH₂), 3.29 (s, 3H), 3.04 (s, 3H), 2.80 (s, 3H).

[(hoz)₂Re(O)(NAr)][B(C₆F₅)₄], Ar = (*p*-OMe)Ph, (**6b**). A round-bottom flask equipped with a magnetic stir bar was charged with [(hoz)₂Re(O)(Solv)][B(C₆F₅)₄], **3**, (0.182 g, 0.146 mmol) dissolved in CH_2Cl_2 . To this solution was added 1 equiv of *p*-methoxy phenyl azide (0.0219 g, 0.147 mmol). The solution was covered and allowed to stir for at least 2 h as it changed color from green to red-orange. The solution was concentrated to approximately 10 mL, and with stirring, 200 mL of pentane were added. A large microcrystalline brown solid appeared. The precipitate was isolated by suction filtration, washed with pentane, and dried under a vacuum to give **6b** in 75% (0.145 g) yield. ¹H NMR (300 MHz, CD₂Cl₂): δ 7.75 (d, 2H, *J* = 8.0 Hz), 7.64 (d, 2H, *J* = 9.1 Hz), 7.32–7.21 (2H, overlapping hoz aromatic), 7.09 (d, 2H, *J* = 9.1 Hz), 6.90–6.78 (2H, overlapping hoz aromatic), 6.29 (d, 1H, *J* = 8.4 Hz, hoz aromatic), 6.18 (d, 1H, *J* = 8.5 Hz, hoz aromatic), 4.97–4.77 (4H, overlapping hoz CH₂), 4.45–4.16 (4H, overlapping hoz CH₂), 4.13 (s, 3H, *p*-OCH₃). ¹³C NMR (200 MHz, CD₂Cl₂): δ 170.8, 170.3, 168.8, 165.2, 163.8, 150.2, 146.6, 145.4, 142.4, 140.4, 138.2, 136.8, 135.6, 133.6, 130.4, 129.4, 128.9, 121.3, 120.3, 120.1, 119.8, 115.0, 110.7, 110.2, 71.4, 71.0, 58.4, 57.3, 55.7. Elemental Analysis Calcd for $C_{49}H_{23}BF_{20}N_3O_6Re$: C, 44.36; H, 1.75; N, 3.17. Found: C, 44.09; H, 1.54; N, 2.92.

Syntheses of Cationic Re(V) Imido Complexes. [(salpd)Re(O)(NMes)(PPh₃)] [B(C₆F₅)₄] (**7**). [(salpd)Re(O)(NMes)][B(C₆F₅)₄], **4**, (0.100 g, 0.077 mmol) was dissolved in CH_2Cl_2 . To this solution was added PPh₃ (0.203 g, 0.77 mmol). The solution changed color from red to green and was stirred overnight. The solvent was removed under a vacuum, and the residue dissolved in a minimal amount of CH_2Cl_2 . Pentane was added until a green powder precipitated. The green powder was washed several times with pentane to yield **7** in 56% (0.066 g) yield. ¹H NMR (300 MHz, CD₂Cl₂): δ 8.09–8.06 (d, 1H, C=N–H), 7.69 (s, 1H, C=N–H), 7.58–7.55 (2H, overlapping aromatic), 7.42–7.2 (16H, overlapping aromatic) 6.95–6.82 (4H, overlapping aromatic), 6.62–6.55 (4H, overlapping aromatic), 4.66–4.63 (1H, saldach CH₂), 4.37–4.36 (m, 1H, saldach CH₂), 4.01–3.98 (m, 1H, saldach CH₂), 3.84 (m, 1H, saldach CH₂), 2.28 (s, 3H, CH₃), 2.15 (s, 6H, CH₃), 1.91 (s, 2H, saldach CH₂). ³¹P (300 MHz, CD₂Cl₂): δ –3.97. Elemental Analysis Calcd for $C_{68}H_{42}BF_{20}N_3O_2PRE$: C, 53.0; H, 2.75; N, 2.73. Found: C, 52.9; H, 2.72; N, 2.89.

[(hoz)₂Re(NAr)(PPh₃)] [B(C₆F₅)₄], Ar = *m*-MeO Phenyl, (**9**). In a typical procedure, a flask equipped with a magnetic stir bar was charged with **3** (0.174 g, 0.139 mmol) dissolved in CH_2Cl_2 . To this solution was added approximately 1 equiv of *m*-methoxy phenyl azide (0.024 g, 0.158 mmol). The solution was covered and allowed to stir overnight as it changed color from green to red/orange. To this solution was added triphenylphosphine (0.394 g, 1.50 mmol). After being stirred for 12 h, the solution became bright green in color. The solution was concentrated to approximately 10 mL. 200 mL pentane were added with stirring.

After an hour a green film was deposited inside the flask. The light green supernatant was removed, and the film redissolved in 10 mL of CH_2Cl_2 . Pentane was added until a green microcrystalline solid was observed. The precipitate was isolated by suction filtration, washed with pentane, and dried under a vacuum to yield **9** in 27% (0.060 g) yield. ¹H NMR (300 MHz, CD₂Cl₂): δ 7.87 (d, 1H, *J* = 8.2 Hz), 7.56–7.20 (18H, overlapping aromatic), 7.06 (d, 2H, *J* = 5.3 Hz), 6.84 (t, 1H, *J* = 7.6 Hz), 6.73 (t, 1H, *J* = 7.3 Hz), 6.62 (dd, 1H, *J* = 7.6 Hz, *J'* = 2.9 Hz), 6.22 (m, 1H), 6.11 (s, 1H), 4.76–4.64 (3H, overlapping hoz CH₂), 4.46–4.29 (2H, overlapping hoz CH₂), 4.16–3.99 (2H, overlapping hoz CH₂), 3.63–3.54 (4H, overlapping hoz CH₂ and *m*-OCH₃). ³¹P NMR (200 MHz, CD₂Cl₂): δ –10.97 (s). Elemental Analysis Calcd for $C_{67}H_{38}BF_{20}N_3O_5PRE$: C, 51.2; H, 2.43; N, 2.67. Found: C, 51.5; H, 2.44; N, 2.43.

Stopped-Flow Kinetics. Equal volumes of solutions of **4–6** in acetonitrile (0.10 mM) and the reductant (PPh₃, PhSMe, or PhSH in excess concentrations 0.02–2.0 M) were mixed in the stopped-flow analyzer at 298 K to give reaction solutions with half the loaded concentrations (50 μM in Re and 0.01–1.0 M in the reducing substrate). The decrease in absorbance of the Re(VII) oxo-imido species was monitored at 500 nm under these pseudo-first-order conditions. The *k_p* values were obtained by nonlinear fitting of Abs₅₀₀ versus time to the equation: Abs_t = Abs_∞ + (Abs₀ – Abs_∞) exp(–*k_pt*). Plots of *k_p* versus [reductant] showed saturation kinetics. Fits of the data to the appropriate rate law, (–d[Re(O)(NAr)⁺]/dt = (*k₄*[LRe(O)(NAr)⁺][Y])/(1/*K₃* + [Y]) (where Y = PAR₃, PhSMe, or PhSH), yielded a first-order rate constant (*k₄*) and an equilibrium constant (*K₃*) for each of the reducing substrates.

¹⁹F NMR Kinetics with 5d. Solutions of **2** (16.6 mM) containing a constant acetonitrile concentration (8.0 M) were prepared in C₆D₆ (1.00 mL), sealed in an NMR tube, and the tube was allowed to equilibrate in the NMR probe at 298 K for at least 10 min. The aromatic azide, *p*-CF₃ phenyl azide, was then added in excess concentration (0.10–0.65 M) to achieve pseudo-first-order conditions. The growth in the integral for the CF₃ signals of the product **5d** (δ –63.5) was monitored over time. Concentrations were determined relative to the ¹⁹F signals of the B(C₆F₅)₄[–] anion, which was used as an internal standard. The *k_p* values were obtained by nonlinear fitting of the data of [5d] versus time to the equation Abs_t = (Abs₀ – Abs_∞)[1 – exp(–*k_pt*)]. A plot of the pseudo-first-order rate constant (*k_p*) versus [*p*-CF₃ phenyl azide] was linear, and the slope afforded an apparent second-order rate constant.

X-ray Structure Determination for 5a. A red dark plate of C₂₉H₃₁N₃O₃Re₂C₂₄BF₂₀ having approximate dimensions of 0.44 × 0.38 × 0.13 mm³ was mounted on a glass fiber in a random orientation. Preliminary examination and data collection were performed with Mo Kα radiation (λ = 0.710 73 Å) on a Nonius KappaCCD equipped with a graphite crystal, incident beam monochromator. Cell constants for data collection were obtained from least-squares refinement, using the setting angles of 29 085 reflections in the range 2° < θ < 27°. The triclinic cell parameters and calculated volume are as follows: *a* = 12.3585(8) Å, *b* = 13.2595(5) Å, *c* = 16.1042(11) Å, α = 106.938(3)°, β = 103.032(3)°, γ = 90.219(3)°, *V* = 2452.6(2) Å³. For *Z* = 2 and FW = 1334.84 the calculated density is 1.81 g/cm³. The refined mosaicity from DENZO/SCALEPACK²⁷ was 0.52° indicating moderate crystal quality. The space group was determined by the program XPREP.²⁸ There were no systematic absences; the space group was determined to be *P*1̄(#2). The data were collected at a temperature of 150(1) K. Data were collected to a maximum 2θ of 55.0°. A total of 29 085 reflections were collected, of which 11 059 were unique. Frames were integrated with DENZO-SMN.²⁷ Lorentz and polarization corrections were applied to the data. The linear absorption coefficient is 26.3 /cm for Mo Kα radiation. An empirical absorption correction using

(27) Otwinowski, Z.; Minor, W. *Methods Enzymol.* **1997**, *276*, 307.

(28) McArdle, P. C. *J. Appl. Crystallogr.* **1996**, *29*, 306.

SCALEPACK²⁷ was applied. Transmission coefficients ranged from 0.642 to 0.720. Intensities of equivalent reflections were averaged. The agreement factor for the averaging was 5.6% based on intensity. The structure was solved using the structure solution program PATTY in DIRDIF99.²⁹ The remaining atoms were located in succeeding difference Fourier syntheses. Hydrogen atoms were included in the refinement but restrained to ride on the atom to which they are bonded. The structure was refined in full-matrix least-squares where the function minimized was $\Sigma w(|F_o|^2 - |F_c|^2)^2$ and the weight w is defined as $1/[\sigma^2(F_o^2) + (0.0501P)^2 + 0.0000P]$ where $P = (F_o^2 + 2F_c^2)/3$. Scattering factors were taken from the "International Tables for Crystallography."³⁰ 11 059 reflections were used in the refinements. However, only the 7982 reflections with $F_o^2 > 2\sigma(F_o^2)$ were used in calculating R1. The final cycle of refinement included 733 variable parameters and converged (largest parameter shift was <0.01 times its sd) with unweighted and weighted agreement factors of $R1 = \Sigma |F_o - F_c|/\Sigma F_o = 0.045$ and $R^2 = \text{SQRT}(\Sigma w(F_o^2 - F_c^2)^2/\Sigma w(F_o^2)^2) = 0.091$. The standard deviation of an observation of unit weight was 1.01. The highest peak in the final difference Fourier had a height of 2.10 e/A³. The minimum negative peak had a height of -1.83 e/A³. Refinement was performed on a LINUX PC using SHELX-97.³¹ Crystallographic drawings were done using programs ORTEP³² and PLUTON.³³

X-Ray Structure Determination for 7. A brown plate of C₄₄H₄₂N₃O₂-PRe, 1.434(CH₂Cl₂), C₂₄BF₂₀ having approximate dimensions of 0.50 × 0.35 × 0.18 mm³ was mounted on a glass fiber in a random orientation. Preliminary examination and data collection were performed with Mo K α radiation ($\lambda = 0.71073 \text{ \AA}$) on a Nonius KappaCCD equipped with a graphite crystal, incident beam monochromator. Cell constants for data collection were obtained from least-squares refinement, using the setting angles of 82 148 reflections in the range $2^\circ < \theta < 27^\circ$. The triclinic cell parameters and calculated volume are as follows: $a = 18.1716(3) \text{ \AA}$, $b = 19.4058(3) \text{ \AA}$, $c = 22.1180(3) \text{ \AA}$, $\alpha = 72.3473(11)^\circ$, $\beta = 76.3375(8)^\circ$, $\gamma = 65.7914(7)^\circ$, $V = 6722.33(18) \text{ \AA}^3$. For $Z = 4$ and $FW = 1662.86$ the calculated density is 1.64 g/cm³. The refined mosaicity from DENZO/SCALEPACK²⁷ was 0.46° indicating good crystal quality. The space group was determined by the program XPREP.²⁸ There were no systematic absences; the space group was determined to be $P\bar{1}(\#2)$. The data were collected at a temperature of 150(1) K. Data were collected to a maximum 2θ of 55.0°. A total of 82 148 reflections were collected, of which 30 634 were unique. Frames were integrated with DENZO-SMN.²⁷ Lorentz and polarization corrections were applied to the data. The linear absorption coefficient is 20.7/cm for Mo K α radiation. An empirical absorption correction using SCALEPACK²⁷ was applied. Transmission coefficients ranged from 0.580 to 0.696. Intensities of equivalent reflections were averaged. The agreement factor for the averaging was 4.9% based on intensity. The

Table 3. Crystal Data and Data Collection Parameters for [(saldach)Re(O)(NMe₃)]₂[B(C₆F₅)₄], **5a**, and [(salpd)Re(NMe₃)(PPh₃)]₂[B(C₆F₅)₄], **7**

	5a	7
formula	C ₅₃ H ₃₁ BF ₂₀ N ₃ O ₃ Re	C _{69.43} H _{44.87} BCl _{2.87} F ₂₀ N ₃ O ₂ PRe
formula weight	1334.84	1662.86
space group	$P\bar{1}$ (no. 2)	$P\bar{1}$ (no. 2)
a , Å	12.3585(8)	18.1716(3)
b , Å	13.2595(5)	19.4058(3)
c , Å	16.1042(11)	22.1180(3)
α , deg	106.032(3)	72.3473(11)
β , deg	103.032(3)	76.3375(8)
γ , deg	90.219(3)	65.7914(7)
V , Å ³	2452.6(2)	6722.33(18)
Z	2	4
ρ_{calc} , g cm ⁻³	1.807	1.643
temp, K	150.	150.
radiation (wavelength)	Mo K α (0.710 73 Å)	Mo K α (0.710 73 Å)
R	0.045	0.053
R_w	0.091	0.124

structure was solved using the structure solution program PATTY in DIRDIF99.²⁹ The remaining atoms were located in succeeding difference Fourier syntheses. Hydrogen atoms were included in the refinement but restrained to ride on the atom to which they are bonded. The structure was refined in full-matrix least-squares where the function minimized was $\Sigma w(|F_o|^2 - |F_c|^2)^2$ and the weight w is defined as $1/[\sigma^2(F_o^2) + (0.0684P)^2 + 0.0000P]$ where $P = (F_o^2 + 2F_c^2)/3$. Scattering factors were taken from the "International Tables for Crystallography."³⁰ 30634 reflections were used in the refinements. However, only the 17 576 reflections with $F_o^2 > 2\sigma(F_o^2)$ were used in calculating R1. The final cycle of refinement included 1847 variable parameters and converged (largest parameter shift was <0.01 times its sd) with unweighted and weighted agreement factors of $R1 = \Sigma |F_o - F_c|/\Sigma F_o = 0.053$ and $R^2 = \text{SQRT}(\Sigma w(F_o^2 - F_c^2)^2/\Sigma w(F_o^2)^2) = 0.124$. The standard deviation of an observation of unit weight was 1.00. The highest peak in the final difference Fourier had a height of 4.03 e/A³. The minimum negative peak had a height of -2.73 e/A³. Refinement was performed on a LINUX PC using SHELX-97.³¹ Crystallographic drawings were done using programs ORTEP³² and PLUTON.³³ A summary of the crystallographic parameters for complexes **5a** and **7** is depicted in Table 3.

Acknowledgment. Support of this work was provided by the Chemical Sciences Division, Office of Basic Energy Sciences, U.S. Department of Energy (Grant No. DE-FG02-06ER15794).

Supporting Information Available: Crystallographic tables for atomic coordinates and equivalent isotropic parameters, bond lengths, and angles for **5a** and **7** (CIF); kinetic profiles, substrate (PAR₃, PhSMe, and PhSH) dependencies for OAT reactions from complexes **4–6**, and Hammett analysis for aryl phosphines (PDF). This material is available free of charge via the Internet at <http://pubs.acs.org>.

JA06551P

- (29) Beurskens, P. T.; Beurskens, G.; Garcia-Granda, R. de G.; Gould, R. O.; Israel, R.; Smits, J. M. M. *The DIRDIF-99 Program System*. Crystallography Laboratory: University of Nijmegen, The Netherlands, 1999.
- (30) *International Tables for Crystallography*; Kluwer Academic Publishers: Utrecht, The Netherlands, 1992; Vol. C, Tables 4.2.6.8 and 6.1.1.4.
- (31) Sheldrick, G. M. *SHELXL97. A Program for Crystal Structure Refinement*; University of Göttingen: Germany, 1997.
- (32) Johnson, C. K. *ORTEP II, Report ORNL-5138*; Oak Ridge National Laboratory: Tennessee, USA, 1976.
- (33) Spek, A. L. *PLUTON. Molecular Graphics Program*; University of Utrecht: The Netherlands, 1991.